

Structural and optical properties of nano-spin coated sol–gel porous TiO₂ films

M. M. EI-NAHASS¹, M. H. ALI², A. EI-DENGLAWEY^{3,4}

1. Physics Department, Faculty of Education, Ain Shams University, Roxy, Cairo 11757, Egypt;
2. Physics Department, Faculty of Science, Ain Shams University, Cairo, Egypt;
3. Physics Department, Faculty of Science, South Valley University, Qena 83523, Egypt;
4. Phys Dep, Fac of Appl Med Sci Turabah, 21995, Taif University, KSA

Received 15 December 2011; accepted 23 May 2012

Abstract: Three thicknesses of TiO₂ films, 174, 195, and 229 nm, were deposited onto quartz substrates by spin coated sol–gel method. The prepared films were characterized by nano-crystalline structure with different crystallite sizes (19–46 nm) and relatively high porous structure. Optical constants were determined and showed the lowest refractive index of 1.66 for the as-prepared films that ever reported till now. Obtained results were discussed through current theoretical ideas.

Key words: TiO₂ films; optical properties; nanostructure; electron microscopy; thin films; spin coating technique

1 Introduction

Many theoretical and experimental investigations have been carried out on the electronic transport properties of semi-conducting oxide thin films. Titanium dioxide or titania, TiO₂, is a high band gap semiconductor that exhibits high transparency to visible and near infra red (NIR) light. It has three crystalline phases: anatase (tetragonal), rutile (tetragonal), and brookite [1–4]. Both anatase and rutile are more common phases than the brookite and have wide commercial applications.

Rutile is the most thermodynamically stable phase of TiO₂. Its refractive index and density are high as compared to anatase phase [5]. Formation of a particular phase depends on the nature of the starting material, its composition, deposition method, and annealing temperatures. TiO₂ is a cheap, harmless, white, and non-biodegradable material. Also, it has high refractive index, high dielectric constant, semiconductor properties and chemical stability. It is widely used in various applications such as optical filters [6], gas sensors [7], ceramic membranes [8], wave-guides [9], photo catalysts [11–14] and dye sensitized solar cells [15]. A number of methods have been employed to prepare TiO₂ films including electron beam evaporation, sputtering,

chemical vapor deposition, laser ablation, polymer technique and sol–gel process [16–21]. The sol–gel process is a liquid-deposit process using soft chemistry, giving homogeneous deposits. It is less demanding in terms of equipment and is thus less costly, and gives the opportunity to deposit films with large surface areas [22,23].

2 Experimental

TiO₂ provided by Millennium inorganic chemicals, SP-300N A Cristal Company, France, was used as the starting material. Three different thicknesses of TiO₂ films, 174, 195, and 229 nm, were prepared with a hand made spin coating at 2500 r/min for 30 s. Film thickness (*d*) was checked by an interferometric method [24]. The specimen of TiO₂ films of 70 nm thickness for TEM examination was prepared on a quartz substrate covered by rock salt. TEM specimen was obtained by removing these films from quartz substrate through water immersing and subsequently, these films were picked up on 200-mesh copper grids of 3.05 mm diameter.

The absorption edge and the refractive index of nano TiO₂ films were determined by reflectance and transmittance spectra performed on the films deposited on quartz substrates by spin coating technique. The quartz substrate was rinsed with acetone and washed

thoroughly with deionized water. The optical measurements were performed by JASCO molel V-570UV-Vis-NIR double beam spectrophotometer in the wavelength range of 200–2500 nm, with a slit width of 3 nm, and a sampling interval of 2 nm. The structure and the optical measurements were performed at room temperature. Structure was analyzed using Philips-CM12 transmission electron microscope (TEM). The reflectance was measured at the normal incidence with an aluminum reference mirror. The absolute values of measured transmittance, T , and reflectance, R , after correcting the absorbance and reflectance of the substrates, are given by [25,26]

$$T = \left(\frac{I_{fr}}{I_q} \right) (1 - R_q) \quad (1)$$

where I_{fr} and I_q are the intensities of the light passing through the film-quartz system and the reference quartz, respectively; R_q is the reflectance of quartz. In addition, if the intensity of light reflected from the sample mirror reaching the detector is I_{fr} and that reflected from the reflectance reference mirror is I_m , then

$$R = \left(\frac{I_{fr}}{I_m} \right) R_m [1 + (1 - R_q)^2] - T^2 R_q \quad (2)$$

where I_m is the intensity of light reflected from the reference mirror, I_{fr} is the intensity of light reflected from the sample reaching the detector and R_m is the mirror reflectance.

Reflectance and transmittance spectra were performed on thin film samples with single face. Extinction coefficient, k and refractive index, n were calculated using T , R and thickness, d , taking into account the experimental error of the film thickness to be $\pm 2\%$ and of T and R to be $\pm 1\%$. The error in the calculated values of n and k are estimated to be $\pm 3\%$ and $\pm 2.5\%$, respectively.

In this work, we have investigated the structure and the optical properties of TiO₂ film because of its various friendly applications. Both n and k of TiO₂ film were determined from the absolute values of the measured transmittance and reflectance at normal light incidence after correcting the absorbance and reflectance of the substrate as given by Eqs. (1) and (2).

3 Results and discussion

3.1 Structural properties

Structural properties of TiO₂ film (70 nm thick) were studied using transmission electron microscope, (TEM). The selected area electron diffraction (SAED)

pattern of the as-deposited TiO₂ films is shown in Fig.1. The corresponding electron diffraction pattern confirms the polycrystalline nature of TiO₂ film. The experimental data show that the TiO₂ film has a tetragonal system (rutile system) with lattice constants of $a=4.53 \text{ \AA}$, $c=2.92 \text{ \AA}$ with $d=2.153, 2.028, 1.656, 1.461 \text{ nm}$ corresponding to Miller indices (111), (210), (211), (002), respectively [27]. The transmission electron microscopy shows nano-crystallites. The size of the observed nano-crystallites was 19–46 nm, as shown in Fig. 2.

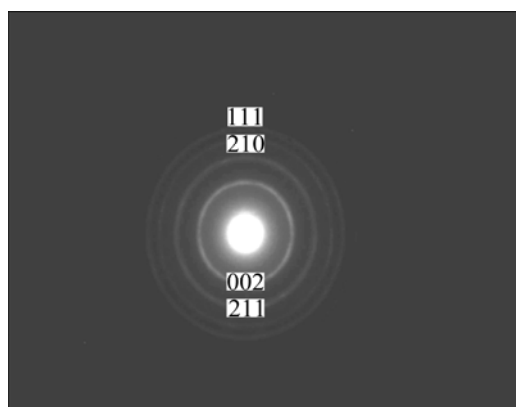


Fig. 1 SAED pattern for TiO₂ film

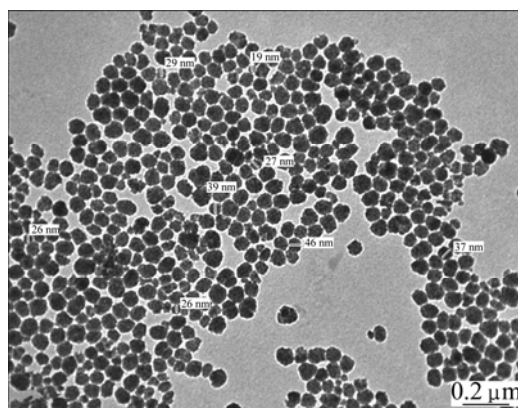


Fig. 2 TEM micrograph for TiO₂ film

3.2 Optical properties

3.2.1 Spectral distribution of T and R

The spectral dependences of T and R of the as-prepared TiO₂ films of three different thicknesses, 174, 195, and 229 nm, are shown in Fig. 3. The results indicate that T increases with the increasing of the incident photons wavelength, λ , and is independent of the film thickness. One can divide the spectral dependences of both T and R of the as-prepared TiO₂ films as a function of λ into two main parts. The first one at $\lambda < 1000 \text{ nm}$ is called high absorption region, and is characterized by drastic change of both T and R as a function of λ in which $T+R < 1$ where the optical constants were determined. The second one is non absorption

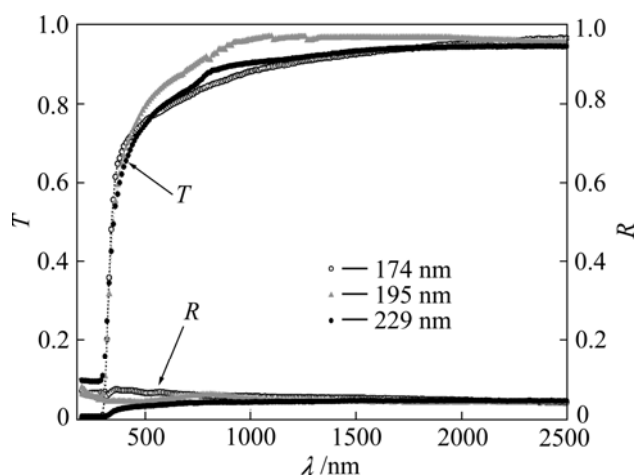


Fig. 3 Dependence of transmission (T) and reflection (R) on wavelength (λ) for TiO_2 films with thicknesses of 174, 195 and 229 nm

region at $\lambda > 1000$ nm; both T and R are characterized by stability through the whole wavelength range of $T+R=1$ where refractive index was determined. Figure 3 announces that the percentage of transmission is approximately 95% in the visible and NIR region consequently, the high transmittance inferred that spin coated TiO_2 films could be used for optical coating applications. The wavelength of the film absorption edge is 290 nm approximately.

3.2.2 Absorption and extinction coefficient

Both of T , R and thickness, d were used to determine the absorption coefficient, α , according to [28]

$$T = (1 - R)^2 \exp(-\alpha d) \quad (3)$$

Optical absorption coefficient (α) is given by

$$\alpha = \frac{1}{d} \ln \frac{(1-R)^2}{T} \quad (4)$$

The calculated absorption coefficient, α , versus photon energy, $h\nu$, is depicted in Fig. 4. One can observe that α increases with the increasing of photon energy through the whole range of high absorption region while it decreases through the non-absorbing region. One can observe that both arrow and circle distinguish the end term of Urbach tail region ($\alpha \leq 10^4 \text{ cm}^{-1}$) and high absorption region ($\alpha \geq 10^4 \text{ cm}^{-1}$). Extinction coefficient of TiO_2 film was calculated by

$$k = \frac{\alpha \lambda}{4\pi} \quad (5)$$

The calculated values of extinction coefficient, k vs λ for TiO_2 films are illustrated in Fig. 5. It could be noticed that k decreases with increasing of λ , and is thickness independent.

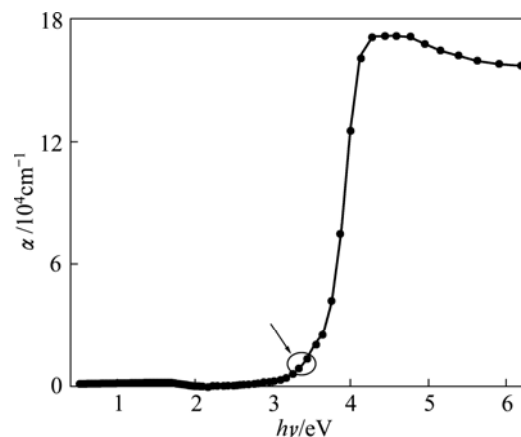


Fig. 4 Absorption coefficient (α) vs photon energy ($h\nu$)

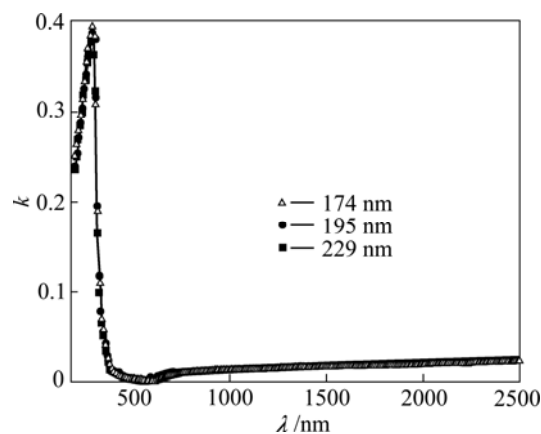


Fig. 5 k vs λ for TiO_2 films with thicknesses of 174, 195 and 229 nm

3.2.3 Optical band gap calculation

An absorption edge of semiconductors corresponds to the threshold of charge transition between the highest nearly filled band and the lowest nearly empty band. According to inter-band absorption theory, the optical band the films of can be calculated using the following relation [29]:

$$\alpha h\nu = A(h\nu - E_{\text{g}}^{\text{opt}})^r \quad (6)$$

where A is the probability parameter for the transition, also the constant A is a measure of the disorder of the material [30], $A = 4\pi\sigma_{\text{min}}/nc\Delta E$, where σ_{min} is the minimum metallic conductivity, n is the refractive index, c is the light-velocity, and $\Delta E = \Delta E_{\text{c}} - \Delta E_{\text{v}}$ represents the band tailing [31]; $E_{\text{g}}^{\text{opt}}$ is the optical band gap of the material, $h\nu$ is the incident photon energy; r is the transition coefficient. The reported value of r is 2 for the measurement of indirect band gap and 1/2 for direct band gap. Both direct and indirect band gaps of TiO_2 films were found, and the indirect optical band gap is evaluated by extrapolating the straight line part of the curves $(\alpha h\nu)^{1/2}$ with energy axes ($h\nu$) i.e. $(\alpha h\nu)^{1/2} = 0$ according to

$$(\alpha hv)^{1/2} = A(hv - E_{gi}^{opt}) \quad (7)$$

Due to phonon energy assisting the indirect transition [32], Eq. (7) could be written as

$$(\alpha hv)^{1/2} = A(hv - E_{gi}^{opt} \pm E_{phonon}) \quad (8)$$

where E_{phonon} is the phonon energy assisting the indirect transition.

Direct optical band gap was evaluated by extrapolating the straight line part of the curves $(\alpha hv)^2$ with energy axes (hv) i.e $(\alpha hv)^2 = 0$ according to

$$(\alpha hv)^2 = A(hv - E_{gd}^{opt}) \quad (9)$$

Relationship of both $(\alpha hv)^2$, $(\alpha hv)^{1/2}$, and hv is depicted in Fig. 6. It reveals the simultaneous existence of direct and indirect band gaps in TiO₂ films.

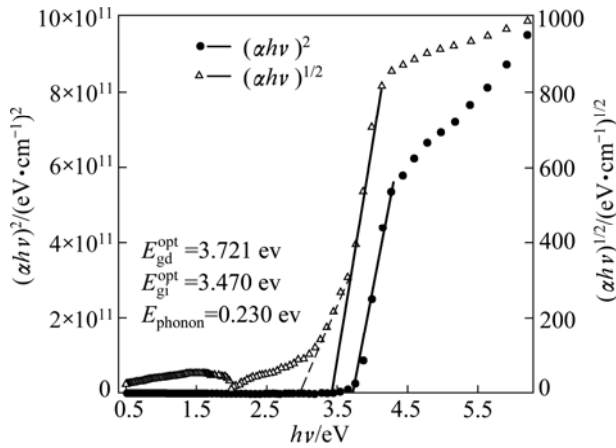


Fig. 6 $(\alpha hv)^2$ and $(\alpha hv)^{1/2}$ vs Photon energy

Values of direct E_{gd}^{opt} , indirect, E_{gi}^{opt} optical band gaps and E_{phonon} were 3.721, 3.47 and 0.230 eV, respectively. Furthermore, the value of indirect band gap was found to be lower than that of direct band gap. Simultaneous existence of a direct, E_{gd}^{opt} and indirect, E_{gi}^{opt} optical band gaps were also reported in Refs. [33–40].

The characters [40–43] augmented our E_{gd}^{opt} and E_{gi}^{opt} results. One can observe that both values of E_{gd}^{opt} and E_{gi}^{opt} are different by ΔE :

$$\Delta E = E_{gd}^{opt} - E_{gi}^{opt} = 3.721 - 3.470 = 0.251 \text{ (eV)}$$

This difference may be attributed to spin orbital splitting [44].

The absorption tail of TiO₂ films was analyzed according to [45]

$$\alpha = \alpha_0 \exp\left(\frac{hv}{E_c}\right) \quad (10)$$

where α_0 is a constant and E_c is the band tail width. The

absorption coefficient is governed by the so-called “Urbach rule”.

Figure 7 shows the plot of $\ln \alpha$ versus hv for TiO₂ films. The released straight line indicates that the absorption threshold characterizes an exponential absorption edge.

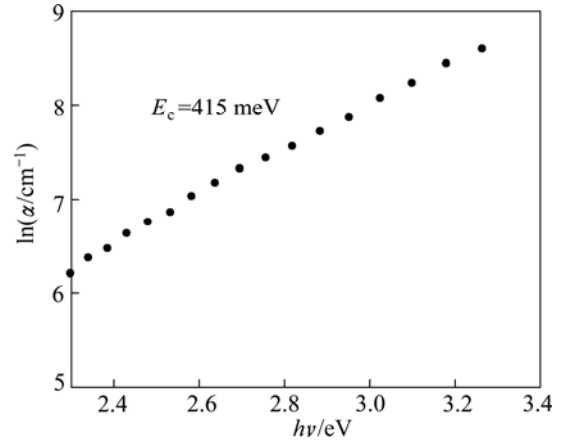


Fig. 7 $\ln(\alpha/\text{cm}^{-1})$ as function of photon energy

The value of E_c for TiO₂ films was 415 meV. To the best of our knowledge no such values of E_c and E_{phonon} in spin coated TiO₂ films have not been previously reported.

It is known that rutile is an oxygen-deficit semi-conducting transition metal oxide at room temperature when equilibrated in an atmosphere of low oxygen activity, and is non-conducting at room temperature when equilibrated in an atmosphere of high oxygen activity [46]. Due to the fact that “the ideal crystal does not exist”, at any temperature crystals contain various structural imperfections or defects. Urbach tail represents the localized states, due to defects in the structure with band tail width of 415 meV. The defect disorder of TiO₂ has generally been considered in terms of oxygen vacancies, titanium interstitials and electrons. The oxygen deficiency introduces an excess of electrons included within bandwidth or the tail of the material. These defects are donor-type defects, therefore TiO₂ has been considered an n-type semi-conductor [47–50]. So, an indirect transition can be seen as a phonon-assisted electronic transition from the maximum of the valence band to the minimum in the conduction band occurring between different points in k -space. Since the valence and conduction band extrema occur at a different k points in the Brillouin zone, the indirect gap excitation requires a phonon to conserve crystal momentum [51] and other optical constants were available elsewhere [44].

3.2.4 Refractive index and dielectric constant

Both R and k at different λ were used to calculate refractive index, n according to [52]

$$n = \frac{1+R}{1-R} + \sqrt{\frac{4R}{(1-R)^2} - k^2} \quad (11)$$

The spectral dependences of both $n(h\nu)$ and $k(h\nu)$ are plotted in Fig. 8. n and k were determined for different film thicknesses. It could be noticed that both n and k are practically independent of film thickness. Therefore, the values used in the plots are the mean values of both n and k . From Fig. 8, one can observe that the tolerance of both n and k lies within the limits of experimental error. The interesting obtained value of n is 1.66 through the wavelength range (300–1200 nm). This is the lowest value reported to the refractive index of the as-prepared spin coated TiO₂ films. The porosity of the films is calculated according to [53]

$$\text{Porosity} = \left(1 - \frac{n^2 - 1}{n_d^2 - 1}\right) \times 100\% \quad (12)$$

where n_d is the refractive index of pore-free anatase ($n_d=2.52$) [54] and n is the refractive index of the porous thin films ($n=1.66$). The calculated porosity was found to equal 67.19%. The lowest value of refractive index ever reported till now is 1.05 for SiO₂ and is 1.67 for TiO₂ [55,56]. The current obtained value of n is so low, it is the lowest value of refractive index ever reported until now for the as- prepared TiO₂ films while the lower value of refractive index ever reported until now of annealed TiO₂ films is reported elsewhere [57].

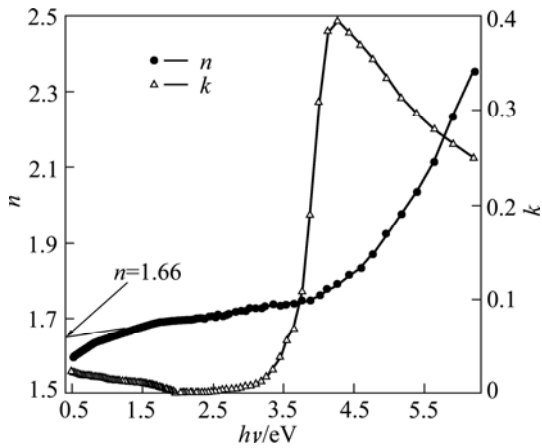


Fig. 8 n and k as function of photon energy

It was reported that the higher refractive indices give an evidence for the fine crystalline of the fabricated films and the correlation between the refractive index and the dielectric constant of a dielectric material. The decrease of the refractive index and packing density can be attributed to the porous structure [16,58]. According to that, the obtained low value of n is attributed to high porous TiO₂ films and nano-crystallites. We can say that

porous density can be engineered in a continuous range of values to obtain low refractive index material. The dispersion of refractive index of TiO₂ films was analyzed using the concept of the single oscillator and could be expressed by the Wemple–DiDomenico (WDD) relationship [59] as

$$(n^2 - 1)^{-1} = -\frac{1}{E_o E_d} (h\nu)^2 + \frac{E_o}{E_d} \quad (13)$$

where $h\nu$ is the photon energy, E_o is the single-oscillator energy and E_d is the dispersion energy which is a measure of the intensity of the inter-band optical transition, and does not depend significantly on the band gap. Plotting $(n^2 - 1)^{-1}$ vs $(h\nu)^2$ shown in Fig. 9 allows to determine the oscillator parameters by fitting a straight line to the experimental points according to Ref. [60]. The obtained values of the single oscillator energy E_o and the dispersion energy E_d were 4.59 and 7.3 eV respectively. By extrapolating the linear part of WDD, optical dispersion relationship towards the infrared spectral region ($h\nu=0$), static refractive index $n(0)$, could be defined by the infinite wavelength dielectric constant ϵ_∞ , which can be deduced to be 2.637. The relationship between the lattice dielectric constant ϵ_L , and the refractive index, n is given by [61]

$$n^2 = \epsilon_L - \left(\frac{e^2}{4\pi^2 \epsilon_o c^2}\right) \left(\frac{N}{m^*}\right) \lambda^2 \quad (14)$$

where ϵ_L is the lattice dielectric constant; N/m^* is the ratio of the carrier concentration to the effective mass; c is the speed of light; e is the electronic charge; ϵ_o is the permittivity of free space.

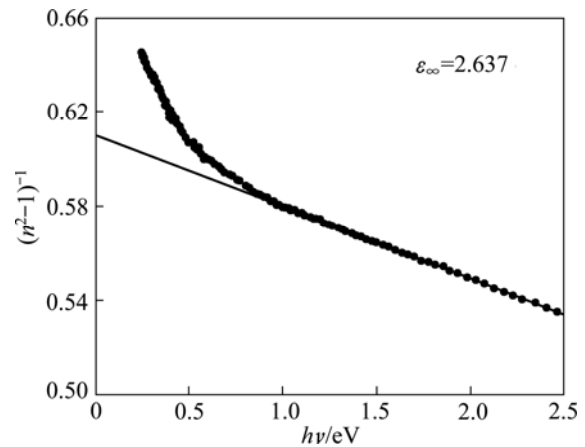


Fig. 9 $(n^2 - 1)^{-1}$ vs $(h\nu)^2$ for TiO₂ film

The plots of n^2 versus λ^2 , are shown in Fig. 10, which is linear verifying of Eq. (14). The value of ϵ_L is determined from the extrapolation of these plots to $\lambda^2 = 0$ and N/m^* from the slope of the graph. The obtained

results are $\epsilon_L=2.769$ and $N/m^* =9.5 \times 10^{37} \text{ kg}^{-1} \cdot \text{m}^{-3}$. The disagreement between the values of ϵ_∞ and ϵ_L may be due to the free carrier concentration [62,63]. The obtained values of n and k were used to calculate both real, ϵ_1 and imaginary part, ϵ_2 of dielectric constant, ϵ :

$$\epsilon = \epsilon_1 - j\epsilon_2, \epsilon_1 = n^2 - k^2 \text{ and } \epsilon_2 = 2nk \tag{15}$$

where ϵ_1 determines the maximum energy that can be stored in the material; ϵ_2 , also is called the relative loss factor, represents the absorption of electrical energy by a dielectric material that is subjected to an alternating electromagnetic field. The loss tangent $\tan \delta$, $\tan \delta = \epsilon_2 / \epsilon_1$, determines how well a material can absorb the electromagnetic field [64], where the angle δ is the phase difference between the applied electric field and the induced current [63]. Figures 11 and 12 show the variation of both ϵ_1 , ϵ_2 and $\tan \delta$ as a function of photon energy. After 2 eV energy value, both ϵ_1 , ϵ_2 and $\tan \delta$ increase forward as the photon energy increases except ϵ_2 and $\tan \delta$ display a maximum starting around 3.7 eV which corresponds to direct energy gap.

3.2.5 Optical conductivity

The optical conductivity is one of the powerful tools for studying the electronic states in materials [65,66]. If a system is subjected to an external electric field, in

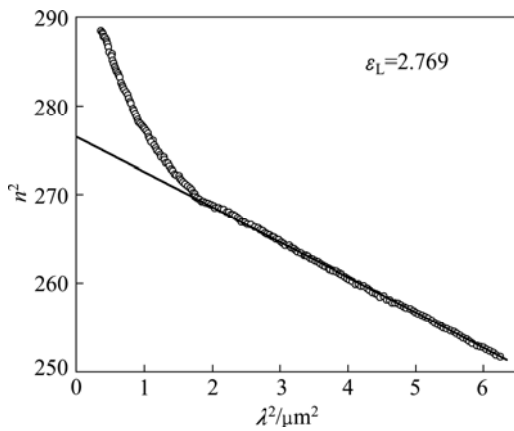


Fig. 10 Plot of n^2 vs λ^2

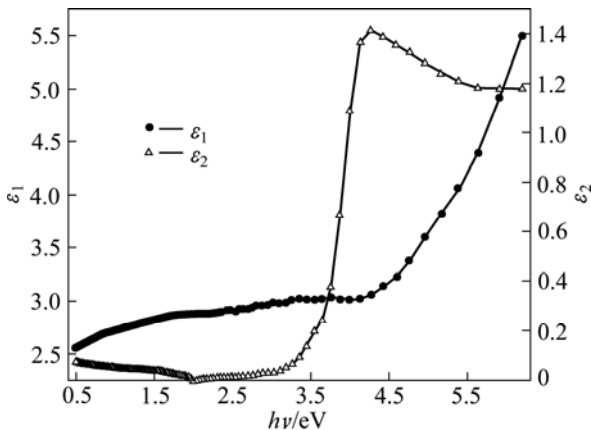


Fig. 11 ϵ_1 and ϵ_2 as function of photon energy

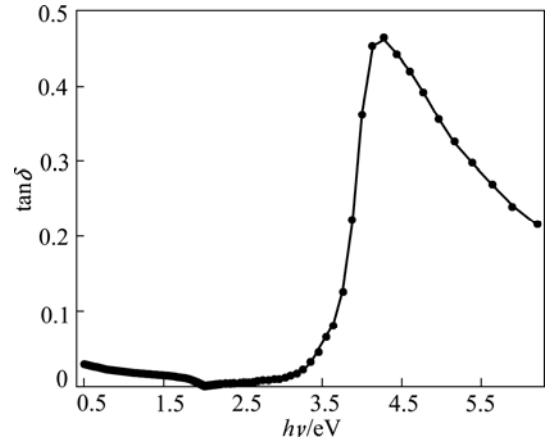


Fig. 12 $\tan \delta$ vs photon energy

general, a redistribution of charges occurs and currents are induced. For small enough fields, the induced polarization and the induced currents are proportional to the inducing field.

The complex optical conductivity, σ is related to the complex dielectric constant, ϵ by [67]

$$\begin{cases} \sigma = \sigma_1 + j\sigma_2 \\ \sigma_1 = \omega \epsilon_2 \epsilon_0 \\ \sigma_2 = \omega \epsilon_1 \epsilon_0 \\ \epsilon = \epsilon_1 + j\epsilon_2 \end{cases} \tag{16}$$

where ω is the angular frequency; ϵ_0 is the free space dielectric constant.

The real, σ_1 and imaginary, σ_2 parts of the optical conductivity dependence of energy are shown in Fig. 13.

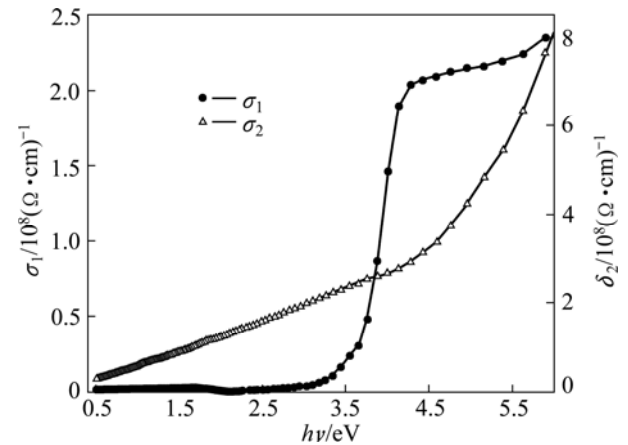


Fig. 13 σ_1 and σ_2 as function of photon energy

It is seen that the optical conductivity increases with increasing photon energy, which has drastically increasing corresponding to the absorption edge and the optical gap. This suggests that the increase in optical conductivity is due to electrons excited by photon energy. The origin of this increasing may be attributed to some changes in the structure due to the charge ordering effect [68].

4 Conclusions

The deposition of TiO₂ was performed on quartz substrates at room temperature in air for three different thicknesses. Structural studies confirm that TiO₂ films have tetragonal system or rutile phase characterized by nanocrystallite size. Optical constants like optical energy gap (direct and indirect) and Urbach tail had been determined to be 3.721 eV, 3.47 eV, and 415 meV, respectively. Indirect optical gap was phonon assisted with energy of 0.230 eV. The difference, ΔE , between values of direct and indirect optical band gap was 0.251 eV and attributes to spin orbital splitting. Low-refractive-index of the as-prepared TiO₂ with the unprecedented refractive index of 1.66 is demonstrated. This low value was attributed to high ratio of porosity (67.19 %) and nano-structure. The obtained values of the oscillator energy, E_0 and oscillator strength, E_d are 7.3 and 4.59 eV, respectively.

The values of the dielectric constant ϵ_∞ , lattice dielectric constant ϵ_L , and the ratio of the carrier concentration to the effective mass and N/m^* are 2.637, 2.769, and $N/m^* = 9.5 \times 10^{37} \text{ kg}^{-1} \cdot \text{m}^{-3}$, respectively. The disagreement between the values of ϵ_∞ and ϵ_L was attributed to the free carrier concentration. The real part of the dielectric constant is higher than the imaginary part through non-absorbing region. The loss tangent, $\tan \delta$ appears to show a drastic increasing at photon energy range of 3.5–4 eV that corresponds to optical energy gap range and absorption energy due to interband transition. Optical conductivity was found to increase as a function of photon energy.

References

- [1] WANG Z, HELMERSSON U, KALL P. Optical properties of anatase TiO₂ thin films prepared by aqueous sol-gel process at low temperature [J]. *Thin Solid Films*, 2002, 405: 50–45.
- [2] SHCHUKIN D G, SVIRIDOV D V, PHOTOCHEM J, PHOTOBIOLOGICAL C. Photocatalytic processes in spatially confined micro- and nan-reactors photochem [J]. *J Photochem Photobiol C: Photochemistry Reviews*, 2006, 7: 23–39.
- [3] ZHANG R, GAO L, ZHANG Q. Photodegradation of surfactants on the nanosized TiO₂ prepared by hydrolysis of the alkoxide titanium [J]. *Chemosphere*, 2004, 54: 405–411.
- [4] RICHARDSON S, THRUSTON A, COLLETTE T, PATTERSON K, LYKINS B. Identification of TiO₂/UV disinfection byproducts in drinking water [J]. *Environ Sci Technol*, 1996, 30: 3327–3334.
- [5] BACH H, KRAUSE D. *Thin films on glass* [M]. Heidelberg: Springer, 1997.
- [6] KOSTLIN H, FRANK G, HEBBINGHAUS G, AUDING H, DENNISSEN K. Optical filters on linear halogen-lamps prepared by dip-coating [J]. *J Non-Cryst Solids*, 1997, 218: 347–353.
- [7] TANG H, PRASAD K, SANJINES R, LEVY F. TiO₂ anatase thin films as gas sensors [J]. *Sens Actuat B*, 1995, 26–27: 71–75.
- [8] YAN Y, CHAUDHURI S R, SARKAR A. Synthesis, characterizations, and optical properties of stacked porous thin films derived from sol-gel process [J]. *J Am Ceram Soc*, 1996, 79: 1061–1065.
- [9] ZHAI J, YANG T, ZHANG L, YAO X. The optical wave guiding properties of TiO₂-SiO₂ composite films prepared by the sol-gel process [J]. *Ceram Int*, 1999, 25: 667–670.
- [10] YU J, ZHAO X, ZHAO Q. Photocatalytic activity of nanometer TiO₂ thin films prepared by the sol-gel method [J]. *Mater Chem Phys*, 2001, 69: 25–29.
- [11] LINSEBIGLER A L, LU G, YATES J T Jr. Photocatalysis on TiO₂ surfaces: Principles, mechanisms, and selected results [J]. *Chem Rev*, 1995, 95: 735–758.
- [12] MILLS A, le HUNTE S. An overview of semiconductor photocatalysis [J]. *J Photochemistry and Photobiology A*, 1997, 108: 1–35.
- [13] LEGRINI O, OLIVEROS E, BRAUN A M. Photochemical processes for water treatment [J]. *Chem Rev*, 1993, 93: 671–698.
- [14] HOFFMANN M R, MARTIN S T, CHOI W, BAHNEMANN D W. Environmental applications of semiconductor photocatalysis [J]. *Chem Rev*, 1995, 95: 69–96.
- [15] KO K H, LEE Y C, JUNG Y J. Enhanced efficiency of dye-sensitized TiO₂ solar cells (DSSC) by doping of metal ions [J]. *J Colloid Interf*, 2005, 283: 482–487.
- [16] WANG S, XIA G, HE H, YI K, SHAO J. Structural and optical properties of nanostructured TiO₂ thin films fabricated by glancing angle deposition [J]. *J Alloys and Compounds*, 2007, 431: 287–291.
- [17] TAKEDA S, SUZUKI S, ODAKA H, HOSONO H. Photocatalytic TiO₂ thin film deposited onto glass by DC magnetron sputtering [J]. *Thin Solid Films*, 2001, 392: 338–344.
- [18] HAH Y, NAM S W, LIM T H, OH I H, HONG S A. Properties of the TiO₂ membranes prepared by CVD of titanium tetraisopropoxide [J]. *J Membr Sci*, 1996, 111: 81–92.
- [19] LIU Pei-sheng, CAI Wei-ping, WAN Li-xi, SHI Ming-da, LUO Xiang-dong, JING Wei-ping. Fabrication and characteristics of rutile TiO₂ nano particles induced by laser ablation [J]. *Transactions of Nonferrous Metals Society of China*, 2009, 19: s743–s747.
- [20] KARTHICK S N, PRABAKAR K, SUBRAMANIA A, JANG J J, KIM HCE-JE. Formation of anatase TiO₂ nanoparticles by simple polymer gel technique and their properties [J]. *Powder Technol*, 2011, 205: 36–41.
- [21] BOUABID K, IHLAL A, AMIR Y, SDAQA A, ASSABBANE A, AIT-ICHOU Y, OUTZOURHIT A, AMEZIANE E L, NOUET G. Optical study of TiO₂ thin films prepared by sol-gel [J]. *Ferroelectrics*, 2008, 372: 69–75.
- [22] BRINKER C J, SCHERER G W. *Sol-gel science* [M]. San Diego, CA: Academic Press, 1990.
- [23] RATH C, MOHANTY P, PANDEY V, MISHRA N C. Oxygen vacancy induced structural phase transformation in TiO₂ nanoparticles [J]. *J Phys D*, 2009, 42: 205101.
- [24] TOLANSKY S. *Multiple beam interferometry of surfaces and films* [M]. London: Oxford University Press, 1988: 147.
- [25] BAKRY A M, EL-NAGGAR A H. Doping effects on the optical properties of evaporated Si:H films [J]. *Thin Solid Films*, 2000, 360: 293–297.
- [26] EL-NAGGAR A H. Optical properties of Al-doped a-Si:H films [J]. *J Phys C: Condensed Matter*, 1999, 11: 9619–1928.
- [27] International Centre for Diffraction Data, JCDS 88—1174.
- [28] EL MANDOUH Z S, SELIM M S. Physical properties of vanadium pentoxide sol gel films [J]. *Thin Solid Films*, 2002, 371: 259–263.
- [29] KIREEV P. *La physics of semiconductors* [M]. Mir ed. Moscow, 1975.

- [30] TAUC J. Amorphous and liquid semiconductors [M]. New York: Plenum, 1976.
- [31] EL-DENGLAWAY A, DONGOL M, EL-NAHASS M M. Photoinduced absorption edge shift of $As_{20}Se_{60}Tl_{20}$ films [J]. *J Lumin*, 2010, 130: 801–804.
- [32] PANKOVE J I. Optical processes on semiconductors [M]. New Jersey: Prentice-Hall, 1971.
- [33] MATHAI C J, SARAVANAN S, ANANTHARAMAN M R, VENKITACHALAM S, JAYALEKSHMI S. Effect of iodine doping on the bandgap of plasma polymerized aniline thin films [J]. *J Phys*, D, 2002, 35: 2206–2210.
- [34] SHAH JALAL A B M, AHMED S, BHUIYAN A H, IBRAHIM M. UV-vis absorption spectroscopic studies of plasma-polymerized m-xylene thin films [J]. *Thin Solid Films*, 1996, 288: 108–111.
- [35] SHARMA T, AGRWAL S, KUMAR S, MITTAL V K, KALSI P C, MANCHANDA V K. Effect of gamma irradiation on the optical properties of CR-39 polymer [J]. *J Mater Sci*, 2007, 42: 1127–1130.
- [36] HIRANKUMAR G, SELVASEKARAPANDIAN S, KUWATA N, KAWAMURA J, HATTORI T. Thermal, electrical and optical studies on the poly(vinyl alcohol) based polymer electrolytes [J]. *J Power Sources*, 2005, 144: 262–267.
- [37] YASAKI Y, SONOYAMA N, SAKATA T. Semiconductor sensitization of colloidal In_2S_3 on wide gap semiconductors [J]. *J Electroanal Chem*, 1999, 469: 116–122.
- [38] JIN M S, KIM N O, KIM G, YOON C S, LEE I C, KIM M Y, KIM W T. Optical properties of undoped and Co_2^{+} -doped CaS, CaSe, BaS, and base single crystals [J]. *J Korean Phys Soc*, 2001, 39: 692–697.
- [39] HASAN M M, HASEEB A S M A, SAIDUR R, MASJUKI H H, HAMDY M. Influence of substrate and annealing temperature on optical properties of RF-sputtered TiO [J]. *Optical Materials*, 2010, 32: 690–695.
- [40] JANITABAR-DARZI S, MAHJOUB A R, NILCHI A. Investigation of structural, optical and photocatalytic properties of mesoporous TiO_2 thin film synthesized by sol-gel templating technique [J]. *Physica E*, 2009, 42: 176–181.
- [41] ELFANAOU A, ELHAMRI E, BOULKADDAT L, IHLAL A, BOUABID K, LAANAB L, TALEB A, Portier X. Optical and structural properties of TiO_2 thin films prepared by sol-gel spin coating [J]. *Int J hydrogen Energy*, 2011, 36: 4130–4133.
- [42] TERESA M, VISEU R, ISABEL M, FERREIRA C. Morphological characterization of TiO_2 thin films [J]. *Vacuum*, 1999, 52: 115–120.
- [43] PARK Y R, KIM K J. Structural and optical properties of rutile and anatase TiO_2 thin films: Effects of co doping [J]. *Thin Solid Films*, 2005, 484: 34–38.
- [44] WAKAKI M, KUDO K, SHIBUYA T. Physical properties and data of optical materials [M]. New York: CRC Press, 2007.
- [45] URBACH F. The long-wavelength edge of photographic sensitivity and of the electronic absorption of solids [J]. *Phys Rev*, 1953, 92: 1324–1324.
- [46] BALACHANDRAN U, N G EROR. Electrical conductivity in non-stoichiometric titanium dioxide at elevated temperatures [J]. *J Mat Sci*, 1988, 23: 2676–2682.
- [47] MATZKE H J. Diffusion in non-stoichiometric oxides [C]// Nonstoichiometric Oxides. SORENSEN O T. New York: Academic Press, 1981.
- [48] KOFSTAD P. Nonstoichiometry, diffusion, and electrical conductivity in binary metal oxides [M]. New York: Wiley-Interscience, 1972.
- [49] NOWOTNY J, BAK T, SORRELL C C, SHEPPARD L R. Materials and devices for energy conversion [M]. Cambridge: Woodhead, 2005: 84–116.
- [50] NOWOTNY M K, BAK T, NOWOTNY J. Electrical properties and defect chemistry of TiO_2 single crystal electrical conductivity [J]. *J Phys Chem B*, 2006, 110: 16270–16282.
- [51] DRESSELHAUS M S. Solid state physics: Part 2—Optical properties of solids. [2012-05-05]. URL: <http://web.mit.edu/course/6/6.732/OldFiles/www/6.732-pt2.pdf>.
- [52] MOSS T S. Optical process in semiconductor [M]. London: Butter Worths, 1959.
- [53] YOLDAS B E, PARTLOW P W. Formation of broad band antireflective coatings on fused silica for high power laser applications [J]. *Thin Solid Films*, 1985, 129: 1–14.
- [54] KINGERY W D, BOWEN H K, UHLMANN D R. Introduction to ceramics [M]. New York: Wiley, 1976.
- [55] XI J Q, SCHUBERT M F, KIM J K, SCHUBERT E F, CHEN M, YULIN S, LIU W, SMART J A. Optical thin-film materials with low refractive index for broadband elimination of Fresnel reflection [J]. *Nature Photonics*, 2007, 1: 176–179.
- [56] SCHUBERT E F, KIM J K, XI J Q. Low-refractive-index materials: A new class of optical thin-film materials [J]. *Phys Stat Sol B*, 2007, 244: 3002–3008.
- [57] NACEUR J B, GAIDI M, BOUSBIH F, MECHIAKH R, CHTOUROU R. Annealing effects on microstructural and optical properties of nanostructured- TiO_2 thin films prepared by sol-gel technique [J]. *Curr Appl Phys*, 2012, 12: 422–428.
- [58] TANEMURAA S, MIAO L, JIN P, KANEKO K, TERAJ A, NABATOVA-GABAIN N. Optical properties of polycrystalline and epitaxial anatase and rutile TiO_2 thin films by rf magnetron sputtering [J]. *Appl Surf Sci*, 2003, 212–213: 654–660.
- [59] WEMPLE S H, DIDOMENICO M. Behavior of the electronic dielectric constant in covalent and ionic materials [J]. *Phys Rev B*, 1971, 3: 1338–1351.
- [60] EL-DENGLAWAY A. Characterization of As-Se-Tl films near infrared region J [J]. *Non-cryst Solids*, 2011, 357: 1757–1763.
- [61] KUMAR G A, THOMAS J, GEORGE N, KUMAR B A, SHNAN P R, NPOORI V P, VALLABHAN C P G, UNNIKRISHNAN N V. Optical absorption studies of free (H_2Pc) and rare earth (RePc) phthalocyanine doped borate glasses [J]. *Phys Chem Glasses*, 2001, 41: 89–93.
- [62] EL-NAHASS M M, DONGOL M, ABOU-ZIED M, EL-DENGLAWAY A. The compositional dependence of the structural and optical properties of amorphous $As_{20}Se_{80-x}Tl_x$ films [J]. *Physica B*, 2005, 368: 179–187.
- [63] EL-NAHASS M M, FARAG A A M, IBRAHIM E M, ABD-EL-RAHMAN S. Structural, optical and electrical properties of thermally evaporated Ag_2S thin films [J]. *Vacuum*, 2004, 72: 453–460.
- [64] NGUYEN V Q, SANGHERA J S, LLOYD I K, AGGARWAL I D, GERSHON D. Room temperature dielectric properties of the $As_{40}S_{(60-x)}Se_x$ glass system [J]. *J Non-cryst Solids*, 2000, 276: 151–158.
- [65] LOSURDO M, GIANGREGORIO M M, LUCHENA M, CAPEZZUTO P, BRUNO G, TORO R G, MALANDRINO G, FRAGALA I L, LO NIGRO R. Structural-optical study of high-dielectric-constant oxide films [J]. *Appl Surf Sci*, 2006, 253: 322–327.
- [66] TOHYAMA T, MAEKAWA S. Effects of carrier-doping on optical conductivity in high T_c copper oxides [J]. *J Phys Soc Jpn*, 1991, 60: 53–56.
- [67] WIKTOREZYK T. Preparation and optical properties of holmium oxide thin films [J]. *Thin Solid Films*, 2002, 405: 238–242.
- [68] KIMURA S, OKUNO M, IWATA H, NISHI T, AOKI H, OCHIAI A. Low-energy optical conductivity of Yb_4As_3 [J]. *Physica B*, 2002, 312–313: 356–358.

溶胶-凝胶旋转涂布法制备的多孔纳米二氧化钛膜的结构和光学性能

M.M. El-NAHASS¹, M. H. ALI², A. El-DENGLAWAY^{3,4}

1. Physics Department, Faculty of Education, Ain Shams University, Roxy, Cairo 11757, Egypt;

2. Physics Department, Faculty of Science, Ain Shams University, Cairo, Egypt;

3. Physics Department, Faculty of Science, South Valley University, Qena 83523, Egypt;

4. Phys Dept Fac of Appl Med Sci Turabah, 21995, Taif University, KSA

摘要: 采用溶胶-凝胶旋转涂布技术在石英基质上沉积三种不同厚度的 TiO₂ 薄膜, 其厚度分别为 174、195 和 229 nm。沉积得到的薄膜是由尺寸为 19~46 nm 的纳米微晶组成的, 并具有较高的多孔结构。测定了薄膜的光学常数, 得到了迄今为止报道的最低折射率 1.66, 并对所得结果进行了讨论。

关键词: TiO₂ 薄膜; 光学性能; 纳米结构; 电子显微镜; 薄膜; 旋转涂布技术

(Edited by YANG Hua)